ACS APPLIED MATERIALS & INTERFACES

Research Article

www.acsami.org

$LiFePO_4$ Nanocrystals: Liquid-Phase Reduction Synthesis and Their Electrochemical Performance

Jie Jiang,[†] Wen Liu,[‡] Jitao Chen,[‡] and Yanglong Hou*,[†]

[†]Department of Materials Science and Engineering, College of Engineering, [‡]College of Chemistry and Molecular Engineering, Peking University, Beijing 100871, China

Supporting Information

ABSTRACT: Nanosized $LiFePO_4$ is a kind of promising material for high performance lithium ion batteries; however, the synthesis of nanosized $LiFePO_4$ still has some challenges in forming an orthorhombic phase in atmospheric liquid phase and protecting the LFP nanoparticles from aggregation, etc. In this work, $LiFePO_4$ nanocrystals were synthesized through a high-temperature (350 °C) liquid-phase reduction method. The size and morphology of nanocrystals can be readily controlled by tuning the ratio of solvents, and the size-dependent behavior of lithium storage performance is also observed. After a carbon-coating surface treatment, rhombic-shaped $LiFePO_4$ nanocrystals display excellent lithium storage properties with high reversible capacities and good cycle life (141.0 mAh g^{-1} at 0.5 C after 50 cycles etc.). This method can be extended to prepare $LiMnPO_4$ nanorods by substituting iron source with manganese salt.

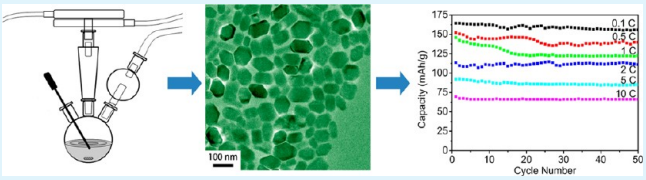

KEYWORDS: *lithium iron phosphate, liquid-phase reduction process, electrochemical performance*

INTRODUCTION

As one of most popular sources of power currently, rechargeable lithium ion batteries (LIBs) have been widely used in portable electrical devices, such as mobiles, tablet computers, video recorders, cameras, and lap tops. Most importantly, with the rapid expense of fossil resources, LIBs have also been regarded as one of the most promising new energies for the new type of transportation tools such as electric vehicles (EVs) and energy storage equipment in recent years because of their unique advantages including low cost, high energy density, and long cycle life.[1−5] To achieve this target, high-quality cathode materials are highly desirable. Among reported cathode materials, $LiFePO_4$ (LFP) has been considered as a promising candidate for the next generation of LIBs with high power and high energy. Compared to the commercial $LiCoO_2$, LFP materials possess a theoretical capacity of 170 mAh g^{-1} and a stable voltage plateau, 3.45 V versus lithium, which is compatible with the window of a solid-polymer Li-ion electrolyte, making LFP have excellent cycle ability and large capacity.[6−9] However, the low electric and ionic conductivities of LFP bulk materials have limited their battery applications to some extent.[10,11] In order to overcome these drawbacks, several strategies have been taken on reducing materials to the nanoscale and controlling their morphology,[12−16] coating the particle's surface with electrically and ionically conductive layers (carbon layers,[17−19] polymer layers,[20,21] or other conductive layers[22]) or enhancing the bulk material's properties,[7,23] etc. So far, various methods have been employed to synthesize LFP materials, such as solid state reaction,[24] sol−gel,[25] hydrothermal,[26−28] coprecipitation,[29] microwave-assisted,[30,31] polyol and solvothermal,[32] micro-emulsion,[33] template mediated,[34] electrospinning,[35] and mechanical activation processes.[36] However, the preparation of LFP nanocrystals still meets some challenges; for example, it is hard to form an orthorhombic phase in atmospheric liquid phase. Iron(II) ion is readily oxidized to hinder the formation of LFP phase, and the aggregation usually occurs due to high surface energy.[36]

Here, we report the synthesis of rhombic-shaped LFP nanocrystals with good crystallinity via a robust, simple high-temperature (350 °C) liquid-phase reduction method, in which the size and morphology of the resulted nanocrystals could be controlled by tuning the solvent ratio and the final performance also showed the size and morphology-dependent behavior. In addition, this synthetic process is a general strategy and can be extended to prepare $LiMnPO_4$ (LMP) nanorods, which have a similar olivine structure with LFP.[30] The high-temperature liquid-phase reduction process involved here is based on oleic acid and oleylamine system,[37−39] which can supply several advantages: (1) offering an experimental environment of high temperature (about 350 °C) under N_2 atmosphere to facilitate the nucleation and growth of well-crystallized LFP materials; (2) oleic acid and oleylamine molecules in the system not only work as the solvent but also serve as the capping and reducing agents to confine the products stable and within nanoscale; (3) providing an opportunity to tune the size and morphology of the products using the synergistic action of these reaction factors such as temperature, time, and controlled processes.

Received: March 8, 2012
Accepted: May 31, 2012
Published: May 31, 2012

After a post carbon-coating process, the carbon-coated LFP nanocrystals exhibit enhanced electrochemical performance and application potential for LIBs.

MATERIALS AND METHODS

Synthesis of $LiFePO_4$ Nanocrystals. The precursor solution was prepared by mixing lithium acetate dehydrate (0.2 mmol, Shanghai Fengshun Fine Chemical Co.), iron(III) acetylacetonate (0.2 mmol, Beijing Yilishiji Co.), and tris(2-ethylhexyl) phosphate (0.2 mmol, Alfa Aesar) with 15 mL of oleic acid (45 mmol, Aldrich) and 15 mL of oleylamine (45 mmol, Aldrich). The mixture was transferred into a three-neck flask system, kept stirring under 70 °C for 10 min to dissolve the reactants, and the solution color changed to dark red. Then the system was degassed under vacuum to remove water and other containing impurities at 120 °C for 1 h. Subsequently, the solution was heated up to 350 °C at the rate of 15 °C min^{-1} under nitrogen atmosphere. It could be seen that the reaction solution remained transparent and dark under 300 °C and rapidly turned to be turbid and brown over 340 °C, indicating the formation of nuclei and growth of nanocrystals. The solution was then kept heating at 350 °C for 1 h, followed by cooling down to the room temperature. The resulted LFP nanocrystals were precipitated upon adding 30 mL of ethanol and collected by centrifugation at 8000 rpm; then they were washed by ethanol and hexane for 5 times to remove the excess surfactants. The final as-synthesized products were dispersed in hexane for further characterization.

Synthesis of $LiMnPO_4$ Nanorods. To obtain LMP nanorods, iron(III) acetylacetonate (0.2 mmol) was substituted with manganese-(II) acetylacetonate (0.2 mmol, Beijing Yilishiji Co.), and the other experimental procedure was just the same as that of LFP nanocrystals.

Carbon-Coating Process. The as-synthesized LFP nanocrystals were mixed with 20 wt % glucose (Beijing Chemical Works) and milled for 1 h. After that, the mixture was transferred into a tube furnace (KMT GSL-1300X) and heated to 600 °C at the rate of 5 °C min^{-1} under argon atmosphere. Subsequently, the mixture was kept at that temperature for 4 h and then allowed to cool to room temperature for further characterization.

Characterizations. X-ray diffraction (XRD) patterns were obtained using a Rigaku DMAX-2400 X-ray diffractometer equipped with Cu Kα radiation. The accelerating voltage and current were 40 kV and 100 mA. The XRD patterns were collected in the 2θ range of 15−70° at a continuous scan mode with step size of 0.02° and scan rate of 4° min^{-1}. FEI Tecnai T20 and F20 were used to get the transmission electron microscope (TEM) and high resolution transmission electron microscope (HRTEM) images of the products. A Hitachi S-4800 was employed to obtain the field-emission scanning electron microscope (SEM) image of the products. A Leeman PROFILE SPEC was used on the inductively coupled plasma (ICP) measurement. Raman spectra was measured on Renishaw SYSTEM 1000 with laser radiation of 632.8 nm. The thermogravimetric and differential thermal analyses (TG-DTA) were determined by a SDT Q600 (USA) in air at a heating rate of 10 °C min^{-1} from room temperature to 700 °C, and X-ray photoelectron spectroscopy (XPS) was obtained with Kartos Axis Ultra with monochromatized Al Kα radiation (1486.6 eV).

Electrochemical Measurements. Electrochemical measurements were performed in two-electrode cells with lithium foil as both reference and counter electrodes. The working electrode consisted of active material, conductive agent (acetylene black), and polymer binder (ploytetrafluoroethylene, PTFE) in a weight ratio of 75:10:15 was pasted onto aluminum foil. A Celgard 2300 membrane was used as a separator. The electrolyte used in the measurement was composed of 1 M $LiPF_6$ solution in ethylene carbonate (EC)/dimethyl carbonate (DMC) (1:1 by volume). Electrodes were prepared in a dry room, and the cells were assembled in an argon-filled glovebox.

The electrochemical performance of these cells was measured on a LAND CT 2001A analyzer (Wuhan Jinnuo) at different current rates with a voltage window of 2.0−4.2 V for LFP and 2.0−4.5 V for LMP at 25 °C, and the cyclic voltammogram (CV) of the cells was measured at room temperature at the scan rate of 0.2 mV s^{-1} on CHI 760C (Shanghai Chenhua).

RESULTS AND DISCUSSION

The chemical structures of the products were characterized by powder XRD analysis. As illustrated in Figure 1, the XRD data

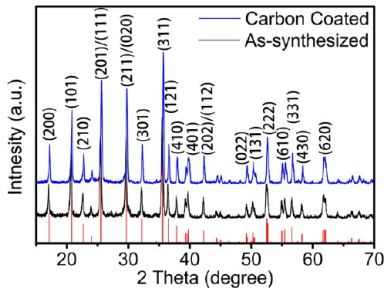

Figure 1. XRD patterns of as-synthesized and carbon-coated LFP nanocrystals.

of the as-synthesized sample is in good agreement with the orthorhombic structure, space group *Pnma* (JCPDS Card No: 83-2092), either the intensity or position of the diffraction peaks, identifying the formation of $LiFePO_4$. The obtained lattice parameters are a = 10.4043 Å, b = 6.0087 Å, and c = 4.7011 Å. The average crystallite size of the sample was calculated to be about 74 ± 1 nm according to the Scherrer equation ($D = 0.89\lambda/\beta\cos\theta$, with β corresponding to the line width at half-maximum corrected for the instrument broadening assuming a Gaussian profile at the angle of diffraction θ and λ corresponding to the X-ray radiation wavelength of 0.154056 nm), suggesting the good crystalline feature of the sample. It should be emphasized that the synthesis of LFP nanocrystals in the current study was performed at a temperature of 350 °C, which is much lower than that of conventional solid state reaction. In other words, our method reported here offers one high efficient route for the synthesis of LFP materials. Moreover, as is well-known, the high temperature solid state reaction usually results in microsized or bulk materials. The carbon-coated sample even after a postcoating process at 600 °C is kept as nanosized material, whose chemical structure is still consistent with typical $LiFePO_4$ with lattice parameters a = 10.2865 Å, b = 5.9936 Å, and c = 4.6828 Å. As identified by XRD data, there is no identical difference in the chemical structure of carbon-coated sample compared to the as-synthesized one. No obvious graphite peaks can be observed in the pattern of carbon-coated sample, neither.

TEM and HRTEM were employed to characterize the shape and morphology of the samples. Figure 2a shows the TEM image of the as-synthesized LFP nanocrystals, displaying monodisperse rhombic shape with an average length of about 80 nm, and the size distribution plot of the as-synthesized ones is illustrated in Figure S1, Supporting Information. The interplanar spacings of 0.350 and 1.035 nm in the HRTEM image of the as-synthesized products (Figure 2b) correspond to (201)/(111) and (100) planes of LFP, suggesting good crystalline state of the sample. Figure 2c is the TEM image of carbon-coated LFP nanocrystals. Compared to Figure 2a, it can be seen from Figure 2c that, after milling with glucose and further heat treatment, there is no big change in the morphology of LFP nanocrystals and the surface of the products is coated with an amorphous carbon layer of about 3

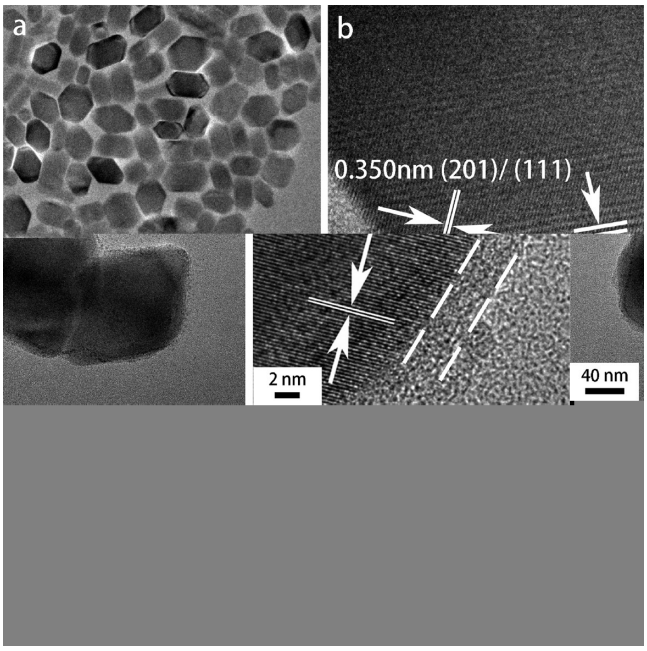

Figure 2. TEM images of (a) as-synthesized and (c) carbon-coated LFP nanocrystals and HRTEM images of (b) as-synthesized and (d) carbon-coated ones.

nm, as shown by the parallel dashed lines in the HRTEM image (Figure 2d). The clear lattice fringes of the LFP nanocrystals exhibit the feature of single crystallinity; the interplanar spacing of 0.300 nm in Figure 2d can be assigned to the (211)/(020) plane of LFP, respectively, which is also in good agreement with the identical peak in the XRD pattern (Figure 1).

It is interesting that the size of LFP nanocrystals could be readily controlled by tuning the ratio of oleic acid to oleylamine in the precursor solution, which is an advantage of the high-temperature liquid-phase reduction process. When the ratio of oleic acid to oleylamine was kept at 1:2, less than 40 nm nanoparticles with poor crystallinity were obtained (Figure S2a, Supporting Information). When the ratio was 1:1, 80 nm rhombic-shaped LFP nanocrystals were obtained (Figure S2b, Supporting Information), while when the ratio was increased to 2:1, the products would be crystals with lengths over several hundred nanometers (Figure S2c, Supporting Information). The XRD patterns of these samples were shown in Figure S3, Supporting Information. In this system, oleic acid and oleylamine worked as both the solvent and surfactants; on the other hand, oleylamine and the short-chain carbon decomposed from both of them served as reducing agent. Note that oleylamine was the critical surfactant with stronger capping effect on the surface of LFP nanocrystals than oleic acid,[40] which mainly influenced the size and morphology of the nanocrystals. Thus, when the oleylamine ratio in the whole solvents was too high, the capping effect was still too strong, even at high temperature, to make the precursors decompose, resulting in the poor-crystallized precipitates. While the oleylamine ratio in the system became low, the capping effect was weaker at the reaction temperature of 350 °C compared to the 1:1 condition, and then the crystals grew larger and the crystallization process took more time.

In order to evaluate the mass ratio of pure LFP in the as-synthesized products, inductively coupled plasma (ICP) spectrometry was recorded. The LFP mass ratios of both samples (shown in Figure S2b,c, Supporting Information) were calculated to be about 70% (Table S1, Supporting Information). The remaining 30% might be the contribution of the surfactants or other impurities that were generated during the synthetic processes and could not be detected by XRD or ICP spectrometry. With the help of the specific surfactants in the reacting mixture, the products showed well-controlled morphology and size-distribution, which were essential to the synthesis and presented performance of nanosized materials.[38] To understand the electrochemical performance of as-synthesized materials, the capacity vs cycle number plots were measured, as shown in Figure S4, Supporting Information. Compared to the others, the 80 nm as-synthesized LFP nanocrystals with good monodispersity display better electrochemical performance,[13] i.e., the reversible capacities of 101.9 mAh g^{-1} at the current of 0.5 C (1 C = 170 mA g^{-1}) after 10 cycles and 81.2 mAh g^{-1} at the current of 2 C after another 10 cycles (Figure S4a, Supporting Information). The crystals over several hundred nanometers give reversible capacities of about 88.5 mAh g^{-1} at the current of 0.5 C after 10 cycles and the following show about 66.0 mAh g^{-1} at the current of 2 C after another 10 cycles (Figure S4b, Supporting Information).

In addition, this simple synthetic strategy can be extended to produce LMP nanorods by the substitution of $Fe(acac)_3$ with $Mn(acac)_2$. As seen in XRD pattern (Figure 3), the LMP samples also have well-crystallized olivine structures (JCPDS Card No: 33-0804) with the lattice parameters a = 10.4043 Å, b = 6.0087 Å, and c = 4.7011 Å. TEM and SEM characterizations indicate that the LMP products possess the rod shape with a size range of 200−300 nm long and about 30 nm in diameter (Figure 4). As shown in Figure S5, Supporting Information, LMP nanorods with a size range of 200−300 nm long and about 30 nm in diameter exhibit reversible capacities of 61.4 mAh g^{-1} at the current rate of 0.5 C (also 1 C = 170 mA g^{-1})

Figure 3. XRD pattern of LMP nanorods.

Figure 4. (a) TEM and (b) SEM images of LMP nanorods.

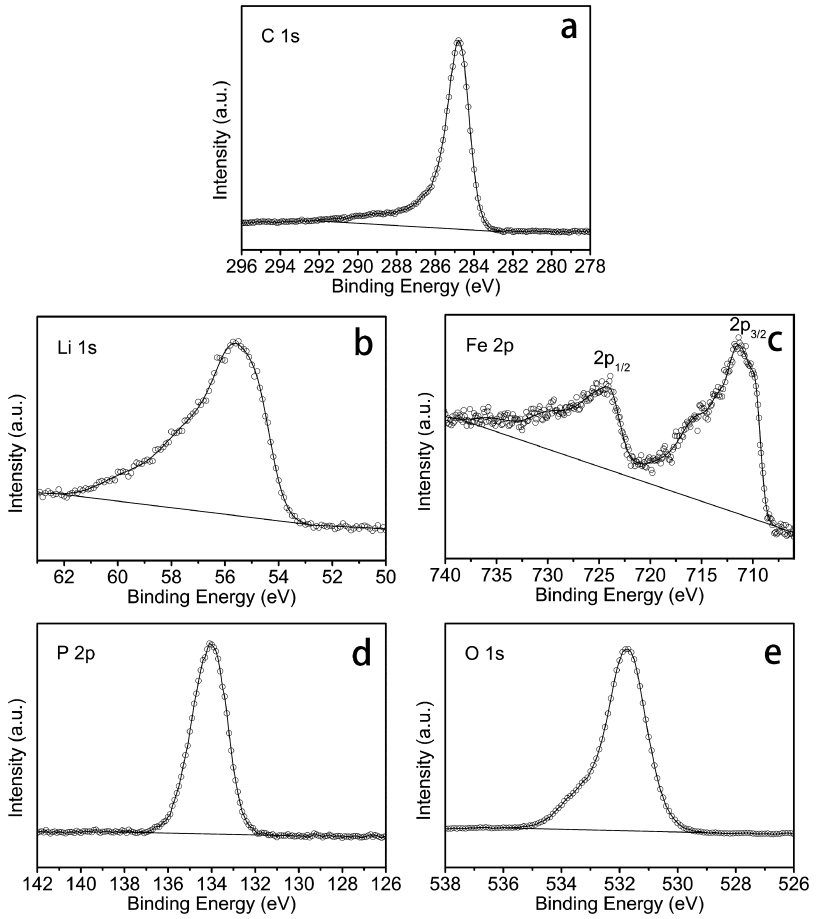

Figure 5. XPS spectra of carbon-coated LFP nanocrystals (a) C 1s, (b) Li 1s, (c) Fe 2p, (d) P 2p, and (e) O 1s.

after 10 cycles and 26.7 mAh g^{-1} at the current of 2 C after another 10 cycles in charge−discharge measurement.

Both the mass ratio and the electrochemical performance of as-synthesized LFP nanocrystals suggested that there were still some capping ligands remaining on the surface of the products, which to some extent decreased the final performance of products.[36,41] In order to improve it, a carbon coating process was introduced. The as-synthesized LFP nanocrystals were milled with 20 wt % glucose for 1 h and then annealed at 600 °C for 4 h under argon atmosphere to get an amorphous carbon layer on the surface of the products. As we expected, after the coating process, the electric and ionic conductivities became better[42] and their performance was correspondingly increased (see below).

To further reveal the chemical structures of the products, X-ray photoelectron spectroscopy (XPS) was therefore employed to evaluate the ion value states of LFP nanocrystals. In the spectra of carbon-coated LFP nanocrystals (Figure 5), the C 1s peak (Figure 5a) at 284.80 eV can be assigned to graphite carbon on the particle surface.[43] The peak at 55.50 eV shown in Figure 5b corresponds to Li 1s, which is consistent with that in the reported literature well,[44] and the binding energy (BE) of 711.40 eV for Fe $2p_{3/2}$ peak (Figure 5c) also matches well with that of Fe^{2+} in LFP.[43,45] For the other elements, the P 2p peak at 134.00 eV (Figure 5d) and the O 1s peak at 531.70 eV (Figure 5e) are assigned to the tetrahedral PO_4 group and O atom bonded with Fe ions, respectively, which are in good agreement with the reported values.[43,45] XPS data also identify the formation of $LiFePO_4$ after the reaction process at the temperature of 350 °C.

Raman spectroscopy has been accepted to be a very versatile, purely optical, high-throughput technique for the characterization of carbon.[22] The situation of coated carbon layer can be characterized by calculating the intensity ratio (I_D/I_G) in Raman spectra of the sample (Figure S6, Supporting Information). The peak at ∼1586 cm^{-1} (G band), arising from emission of zone-center optical phonons, corresponds to the doubly degenerate E2g mode of graphite related to the vibration of sp^2-bonded carbon atoms. The disorder-induced D band is assigned to the peak of 1334 cm^{-1}. The I_D/I_G ratio is calculated to be 1.02, showing that there is almost the same amount of disordered and graphitized carbon in the forming carbon layer, and the glucose molecules are not totally graphitized after the heat treatment.

To clarify the mass ratio of the coated carbon on the surface of final products, the thermogravimetric (TG) data were measured. As seen in Figure 6, in a typical TG-DTA process, the sample was heated in air from room temperature to 700 °C at the rate of 10 °C min^{-1}. For pure LFP, the oxidation equation is as follows,[17,46]

$$LiFePO_4 + 1/4O_2 \rightarrow 1/3Li_3Fe_2(PO_4)_3 + 1/6Fe_2O_3 \quad (1)$$

With the existence of carbon component, the total oxidation equation for the carbon-coated LFP nanocrystals is transformed to eq 2,[17,46]

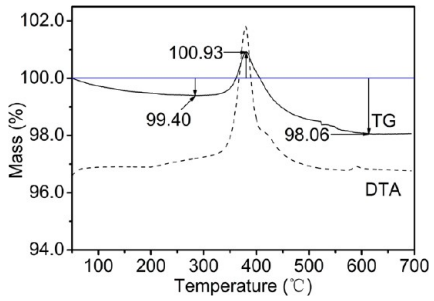

Figure 6. TG-DTA plots of the carbon-coated LFP nanocrystals.

$$LiFePO_4 + xC + (x + 1/4)O_2 \rightarrow 1/3Li_3Fe_2(PO_4)_3 + 1/6Fe_2O_3 + xCO_2 \quad (2)$$

According to eq 2, the mass ratio of the carbon layer could be estimated from the weight change in the heating process. It should be mentioned that the carbon-coated LFP nanocrystals lost a little weight at the starting part of the heating process due to the absorbed water evaporation, and then $LiFePO_4$ component started to be oxidized at about 320 °C which caused the mass increase of the sample.[17,46] At about 380 °C, the carbon layer started to be oxidized to CO_2 gas and the sample began to lose weight.[17,46] When the temperature reached 600 °C, the oxidizing reaction of the sample completed and the mass was kept constant. Thus, from the TG-DTA data of the carbon-coated LFP nanocrystals, the mass ratio of the carbon layer in the products is calculated to be 6.10 wt %. The calculation process is shown in eq 3. This ratio is ideal for promoting the electron transfer efficiency of the products.[42]

$$157.7 + mC = (417.7/3 + 159.6/6) \times 98.06/99.40$$
$$mC = 10.3 \qquad C\% = mC/(mC + 157.7) = 6.10\ wt\ \% \quad (3)$$

To examine the electrochemical performance of carbon-coated LFP nanocrystals, the cyclic voltammogram (CV) curve was first measured at room temperature (Figure S7, Supporting Information). The major anodic/cathodic peaks between 3.25 and 3.75 V are assigned to the redox couple and structural transformations of $Fe^{2+/3+}$ ($LiFePO_4 \leftrightarrow Li^+ + FePO_4 + e^-$), which is also a typical LFP redox property.[47] The CV also indicates no obvious impurity formed in the synthetic process.

To further understand the electrochemical performance of carbon-coated LFP nanocrystals, the galvanostatic charge–discharge curves of the samples for the 50th cycle were measured. As seen in Figure 7, the charge plateaus, originating from the reaction $LiFePO_4 \rightarrow Li^+ + FePO_4 + e^-$, shift from 3.5 V to nearly 3.7 V with the increasing current rates, as the corresponding discharge plateaus, originating from the reaction $Li^+ + FePO_4 + e^- \rightarrow LiFePO_4$, shifting from about 3.4 V to nearly 3.2 V. The increasing voltage differences between the charge and discharge plateaus indicate the increasing incompleteness of the charge–discharge processes with the current rate ranging from 0.1 to 10 C, which also leads to the specific different discharge capacities as discussed below. As the plots show, all the samples give good reversibility at the 50th cycle at different rates, from 0.1 to 10 C. As for the discharge capacity, interestingly, the electrode containing carbon-coated LFP nanocrystals exhibit a discharge capacity of 155.7 mAh g^{-1} at a current rate of 0.1 C, which is about 91.6% of its theoretical capacity of 170 mAh g^{-1},[44] suggesting that the carbon-coated LFP nanocrystals possess a rather high capacity according to the reported value.[32]

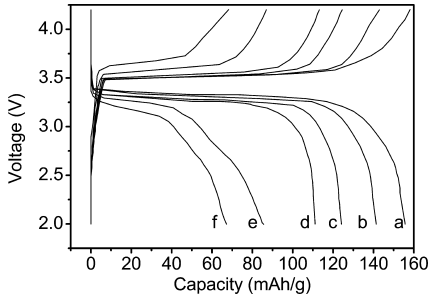

Figure 7. Galvanostatic charge–discharge curves of carbon-coated LFP nanocrystals for the 50th cycle at various charge–discharge rates (a) 0.1 C, (b) 0.5 C, (c) 1 C, (d) 2 C, (e) 5 C, and (f) 10 C.

The plots of specific discharge capacities versus the cycle number at different current rates are shown in Figure 8. It can be seen that the carbon-coated LFP nanocrystals give an initial discharge capacity of 162.4 mAh g^{-1} and remain a capacity of 155.7 mAh g^{-1} after 50 cycles at the current rate of 0.1 C, which is consistent with that in Figure 7. At the current of 0.5 C, the sample shows a reversible capacity of 140.9 mAh g^{-1} after 50 cycles which is still 91.0% of the initial cycle value, and compared with the as-synthesized ones (Figure S3, Supporting Information), the capacity is enhanced by about 37% (from 101.2 to 140.9 mAh g^{-1}), which is a great achievement of the carbon-coating process. The sample displays a capacity of 121.8 mAh g^{-1}, which is 83.5% of the initial cycle value after 50 cycles at the current rate of 1 C. At higher current rates, the LFP nanocrystals show reversible capacities of 110.0 mAh g^{-1} at the current of 2 C, which also increase a lot compared to the as-synthesized ones, and give about 85.0 mAh g^{-1} at 5 C after 50 cycles (Figure 8), and remain a capacity of 66.7 mAh g^{-1} at 10 C even after 80 cycles, as shown in Figure S8, Supporting Information. These results demonstrate the cycle stabilities and good retentions of the carbon-coated LFP nanocrystals. Moreover, the Columbic efficiency (the ratio of charge capacity to discharge capacity) for the sample's first cycle is 102.2% and remains 101% over all the 50 cycles (Figure 9), indicating a good reversibility. The smaller particle size of the sample and coated carbon may contribute to the better charge and discharge capabilities, which may arise from the enhanced contact area between the LFP cathode and the electrolytes.[44]

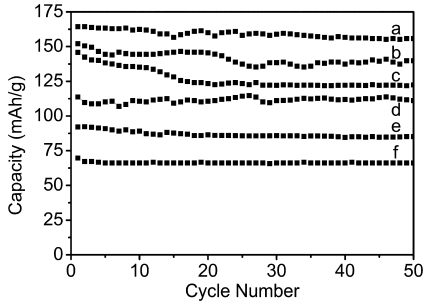

Figure 8. Discharge capacity vs cycle number plots of carbon-coated LFP nanocrystals at various charge–discharge rates (a) 0.1 C, (b) 0.5 C, (c) 1 C, (d) 2 C, (e) 5 C, and (f) 10 C.

It should be mentioned that, compared to as-synthesized sample, the carbon-coated LFP nanocrystals exhibit excellent

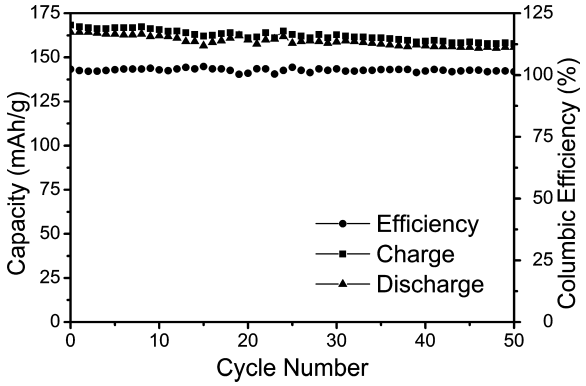

Figure 9. Capacity vs cycle number and Columbic efficiency plots of carbon-coated LFP nanocrystals at the current of 0.1 C.

electrochemical efficiencies and can display good lithium storage performance at different charge−discharge current rates, from low (0.1 C) to high (10 C), it means that their electrochemical performance is greatly enhanced after the simple carbon-coating process (about 37% at 0.5 C, etc.),[42] showing great potential application in the LIBs.[36] On the other hand, the discharge performance of carbon-coated LFP nanocrystals at high rates is relatively poor, which reminds us that the electronic conductivity and lithium-ion diffusion coefficient should be further improved in our next step, although both of them are the intrinsic problems of LFP materials.

CONCLUSIONS

In conclusion, $LiFePO_4$ nanocrystals with good crystallinity, controllable size, and morphology can be synthesized by tuning the solvent composition via a new high-temperature liquid-phase reduction process. Among them, the 80 nm rhombic-shaped LFP nanocrystals exhibit the best original capacities. With the enhancement of electric and ionic conductivities by the carbon layers, the carbon-coated LFP nanocrystals display better reversible capacities at different charge−discharge current rates (from 0.1 to 10 C, e.g., the capacities at the current of 0.1 C is 155.7 mAh g^{-1}). This work offers one simple and robust route to prepare $LiFePO_4$ nanocrystals, which can be extended to other materials, such as $LiMnPO_4$, for next generation high power and performance of LIBs.

ASSOCIATED CONTENT

Supporting Information

Figure S1 shows the histogram of particle size distribution of as-synthesized LFP nanocrystals. Figure S2 give the TEM images of LFP nanocrystals synthesized in different solvent ratio. The XRD patterns of these sample is shown in Figure S3. Capacity vs cycle number plots of as-synthesized LFP nanocrystals and LMP nanorods are shown in Figures S4 and S5. Figure S6 present the Raman spectra of carbon-coated LFP nanocrystals. Cyclic voltammogram of carbon-coated LFP nanocrystals is shown in Figure S7. Figure S8 gives the capacity vs cycle number plots of carbon-coated LFP nanocrystals at the current of 10 C.This material is available free of charge via the Internet at http://pubs.acs.org.

AUTHOR INFORMATION

Corresponding Author

*E-mail: hou@pku.edu.cn.

Notes

The authors declare no competing financial interest.

ACKNOWLEDGMENTS

This work was financially supported by NSFC (51125001, 51172005, 90922033), the National High-tech R&D Program of China (863 Program) (2009AA035201), the Doctoral Program (20090001120010) and New Century Talent of the Education Ministry of China (NCET-09-0177), Yok Ying Tung Found (122043), Beijing Outstanding Talent Program (2009D013001000013), and New Star Program of BCST (2008B02).

REFERENCES

(1) Armand, M.; Tarascon, J.-M. *Nature* **2008**, *451*, 652−657.
(2) Tarascon, J.-M.; Armand, M. *Nature* **2001**, *414*, 359−367.
(3) Winter, M.; Besenhard, J. O.; Spahr, M. E.; Novak, P. *Adv. Mater.* **1998**, *10*, 725−763.
(4) Kang, K.; Meng, Y. S.; Breger, J.; Grey, C. P.; Ceder, G. *Science* **2006**, *311*, 977−980.
(5) Kang, B.; Ceder, G. *Nature* **2009**, *458*, 190−193.
(6) Padhi, A. K.; Nanjundaswamy, K. S.; Goodenough, J. B. *J. Electrochem. Soc.* **1997**, *144*, 1188−1194.
(7) Chung, S.-Y.; Bloking, J. T.; Chiang, Y.-M. *Nat. Mater.* **2002**, *1*, 123−128.
(8) Herle, P. S.; Ellis, B.; Coombs, N.; Nazar, L. F. *Nat. Mater.* **2004**, *3*, 147−152.
(9) Yamada, A.; Koizumi, H.; Nishimura, S.-I.; Sonoyama, N.; Kanno, R.; Yonemura, M.; Nakamura, T.; Kobayashi, Y. *Nat. Mater.* **2006**, *5*, 357−360.
(10) Delacourt, C.; Laffont, L.; Bouchet, R.; Wurm, C.; Leriche, J.-B.; Morcrette, M.; Tarascon, J.-M.; Masquelier, C. *J. Electrochem. Soc.* **2005**, *152*, A913−A921.
(11) Morgan, D.; Van der Ven, A.; Ceder, G. *Electrochem. Solid State Lett.* **2004**, *7*, A30−A32.
(12) Yang, H.; Wu, X.-L.; Cao, M.-H.; Guo, Y.-G. *J. Phys. Chem. C* **2009**, *113*, 3345−3351.
(13) Arico, A. S.; Bruce, P.; Scrosati, B.; Tarascon, J.-M.; Van Schalkwijk, W. *Nat. Mater.* **2005**, *4*, 366−377.
(14) Kobayashi, G.; Nishimura, S.-I.; Park, M.-S.; Kanno, R.; Yashima, M.; Ida, T.; Yamada, A. *Adv. Funct. Mater.* **2009**, *19*, 395−403.
(15) Guo, Y.-G.; Hu, J.-S.; Wan, L.-J. *Adv. Mater.* **2008**, *20*, 2878−2887.
(16) Fisher, C. A. J.; Islam, M. S. *J. Mater. Chem.* **2008**, *18*, 1209−1215.
(17) Belharouak, I.; Johnson, C.; Amine, K. *Electrochem. Commun.* **2005**, *7*, 983−988.
(18) Yuan, S. M.; Li, J. X.; Yang, L. T.; Su, L. W.; Liu, L.; Zhou, Z. *ACS Appl. Mater. Interfaces* **2011**, *3*, 705−709.
(19) Sinha, N. N.; Shivakumara, C.; Munichandraiah, N. *ACS Appl. Mater. Interfaces* **2010**, *2*, 2031−2038.
(20) Huang, Y.-H.; Goodenough, J. B. *Chem. Mater.* **2008**, *20*, 7237−7241.
(21) Lepage, D.; Michot, C.; Liang, G.; Gauthier, M.; Schougaard, S. B. *Angew. Chem., Int. Ed.* **2011**, *50*, 6884−6887.
(22) Zhou, X.; Wang, F.; Zhu, Y.; Liu, Z. *J. Mater. Chem.* **2011**, *21*, 3353−3358.
(23) Wang, L.; Li, Z.; Xu, H.; Zhang, K. *J. Phys. Chem. C* **2008**, *112*, 308−312.
(24) Delmas, C.; Maccario, M.; Croguennec, L.; Le Cras, F.; Weill, F. *Nat. Mater.* **2008**, *7*, 665−671.
(25) Dominko, R.; Bele, M.; Gaberscek, M.; Remskar, M.; Hanzel, D.; Goupil, J. M.; Pejovnik, S.; Jamnik, J. *J. Power Sources* **2006**, *153*, 274−280.
(26) Sun, C.; Rajasekhara, S.; Dong, Y.; Goodenough, J. B. *ACS Appl. Mater. Interfaces* **2011**, *3*, 3772−3776.

(27) Ellis, B.; Kan, W. H.; Makahnouk, W. R. M.; Nazar, L. F. *J. Mater. Chem.* **2007**, *17*, 3248−3254.
(28) Sun, C.; Rajasekhara, S.; Goodenough, J. B.; Zhou, F. *J. Am. Chem. Soc.* **2011**, *133*, 2132−2135.
(29) Delacourt, C.; Poizot, P.; Levasseur, S.; Masquelier, C. *Electrochem. Solid State Lett.* **2006**, *9*, A352−A355.
(30) Murugan, A. V.; Muraliganth, T.; Ferreira, P. J.; Manthiram, A. *Inorg. Chem.* **2009**, *48*, 946−952.
(31) Murugan, A. V.; Muraliganth, T.; Manthiram, A. *J. Phys. Chem. C* **2008**, *112*, 14665−14671.
(32) Rangappa, D.; Sone, K.; Kudo, T.; Honma, I. *J. Power Sources* **2010**, *195*, 6167−6171.
(33) Myung, S.-T.; Komaba, S.; Hirosaki, N.; Yashiro, H.; Kumagai, N. *Electrochim. Acta* **2004**, *49*, 4213−4222.
(34) Lim, S.; Yoon, C. S.; Cho, J. *Chem. Mater.* **2008**, *20*, 4560−4564.
(35) Hosono, E.; Wang, Y.; Kida, N.; Enomoto, M.; Kojima, N.; Okubo, M.; Matsuda, H.; Saito, Y.; Kudo, T.; Honma, I.; Zhou, H. *ACS Appl. Mater. Interfaces* **2010**, *2*, 212−218.
(36) Julien, C. M.; Mauger, A.; Zaghib, K. *J. Mater. Chem.* **2011**, *21*, 9955−9968.
(37) Xu, Z.; Shen, C.; Hou, Y.; Gao, H.; Sun, S. *Chem. Mater.* **2009**, *21*, 1778−1780.
(38) Zeng, Y.; Hao, R.; Xing, B.; Hou, Y.; Xu, Z. *Chem. Commun.* **2010**, *46*, 3920−3922.
(39) Hou, Y.; Xu, Z.; Sun, S. *Angew. Chem., Int. Ed.* **2007**, *46*, 6329−6332.
(40) Park, J.; An, K.; Hwang, Y.; Park, J.-G.; Noh, H.-J.; Kim, J.-Y.; Park, J.-H.; Hwang, N.-M.; Hyeon, T. *Nat. Mater.* **2004**, *3*, 891−895.
(41) Dominko, R.; Goupil, J. M.; Bele, M.; Gaberscek, M.; Remskar, M.; Hanzel, D.; Jamnik, J. *J. Electrochem. Soc.* **2005**, *152*, A858−A863.
(42) Pan, F.; Wang, W.-l.; Chen, D.; Yan, W. *J. Mater. Chem.* **2011**, *21*, 14680−14684.
(43) Rho, Y.-H.; Nazar, L. F.; Perry, L.; Ryan, D. *J. Electrochem. Soc.* **2007**, *154*, A283−A289.
(44) Saravanan, K.; Reddy, M. V.; Balaya, P.; Gong, H.; Chowdari, B. V. R.; Vittal, J. J. *J. Mater. Chem.* **2009**, *19*, 605−610.
(45) Caballero, A.; Cruz-Yusta, M.; Morales, J.; Santos-Pena, J.; Rodriguez-Castellon, E. *Eur. J. Inorg. Chem.* **2006**, *9*, 1758−1764.
(46) Lou, X.; Zhang, Y. *J. Mater. Chem.* **2011**, *21*, 4156−4160.
(47) Palomares, V.; Goni, A.; de Muro, L. G.; de Meatza, I.; Bengoechea, M.; Miguel, O.; Rojo, T. *J. Power Sources* **2007**, *171*, 879−885.